AIAA JOURNAL
Vol. 49, No. 3, March 2011

Excitation of a Zero Mass Flow Liner for Acoustic Damping

C. Lahiri,* B. Pardowitz,† and F. Bake‡
DLR, German Aerospace Center, 10623 Berlin, Germany
I. Röhle§
DLR, German Aerospace Center, 37073 Göttingen, Germany
and
L. Enghardt¶
DLR, German Aerospace Center, 10623 Berlin, Germany

DOI: 10.2514/1.J050421

The zero mass flow liner concept is able to convert a perforated liner with minimal damping qualities into a very effective sound absorber. The damping improvement results from an additional acoustic excitation within the zero mass flow liner. This paper studies the damping performance of the zero mass flow liner while changing the parameters of this excitation. A strong dependency on the sound pressure level and frequency is revealed from the experiments. A mode structure with a distinct pressure pattern seems to be of minor importance. However, it is of great benefit to operate the actuator at its natural resonances. This leads to a very good damping performance at a comparatively low input power.

I. Introduction

THE zero mass flow liner (ZMFL) is a novel concept to enhance the damping performance of a perforated liner with a bias flow. It was shown before [1–5] that a steady bias flow applied to a perforated liner can improve its damping performance considerably. The ZMFL achieves similar results with an unsteady, oscillating bias flow. The advantage of the ZMFL is that it does not need any additional air supply. The unsteady bias flow can be generated entirely by the available fluid, so that the net mass flow rate is zero.

Figure 1 shows a basic ZMFL setup connected to a duct. An acoustic wave p is propagating in the duct from the left to the right. An acoustic actuator, e.g., a loudspeaker, excites an additional sound field p_a inside the cavity behind the perforation. The oscillating bias flow $\tilde{u}$ is produced if the amplitude of the actuator sound field is sufficiently high. The existence of the oscillating bias flow improves the damping of the sound wave p passing the ZMFL in the duct.

First experimental results with this novel concept were presented by the authors at the AIAA Aeroacoustics Conference in 2008 [6]. This included a comparison between a perforated liner with a steady and unsteady bias flow. Both configurations revealed similar damping characteristics, suggesting that the underlying physical effects responsible for the absorption are the same in both cases. The steady bias flow setup has been treated by several authors. Theoretical analyses [7–9] see the generation of vortices as the main mechanism by which sound energy is dissipated. It is assumed that the acoustic energy is converted into kinetic energy of the vortices and subsequently dissipated into heat. The bias flow enables the vorticity shedding and creates a foundation for this energy transfer. The unsteady bias flow of the ZMFL seems to produce a very similar effect.

The unsteady bias flow is generated by a nonlinear interaction between the high-amplitude actuator sound field and the orifices of the liner. It can be assumed that the actuator sound field produces an unsteady bias flow through the orifices if its amplitude is sufficiently high. The generation of such hydrodynamic flows by high-amplitude sound could already be observed in several studies in the past. Ingard and Labate [10] have studied the nonlinear interaction at an orifice. They carried out a visual study of the flow structures in the vicinity of the orifice and defined four regions corresponding to different intensities of the incident sound. In region four, the high-sound-intensity region, they observed the formation of jets and vortex rings symmetrically on both sides of the orifice. Later, Ingard and Ising [11] did simultaneous measurements of the flow velocity in the orifice and the acoustic pressure fluctuations producing the flow. For large amplitudes they found a square-law relation between the pressure and velocity amplitudes. Schlieren photographs by Whiffen and Ahuja [12] and Salikuddin and Brown [13,14] document jet formation and vorticity shedding due to high-intensity sound incident on duct terminations of various forms (nozzles, orifice plates, and perforated plates). Numerical studies by Tam and Kurbatskii [15] and Tam et al. [16] show vorticity shedding for high sound pressure levels at the openings of resonant liners. All of these studies examine the dissipation of acoustic energy caused by the nonlinear interaction between the sound wave and the orifice. The ZMFL makes use of the nonlinear interaction only to generate an unsteady bias flow. Then, the effect of the unsteady bias flow on the test signal propagating in the duct is investigated, while the amplitude of the test signal is in the linear regime.

In flow control applications zero net mass flow jets are known as synthetic jets. Glezer and Amitay [17] give an comprehensive overview on the subject. The unique feature of synthetic jets is that they are formed entirely from the working fluid. They can be generated by placing an oscillating diaphragm or piston behind an orifice and thus force the alternating suction and ejection of fluid across the orifice. Furthermore, acoustic fields of high amplitude have been used to produce the jets, similar to the ZMFL. However, up to now the concept of synthetic jets has not been used in acoustic damping applications.

The ZMFL should not be mistaken for an active noise control system. An active noise control system relies on the destructive interference of two signals at the same frequency with an inverted

Presented as Paper 2009-3110 at the 15th AIAA/CEAS Aeroacoustic Conference, Miami, FL, 11–13 May 2009; received 8 January 2010; revision received 30 July 2010; accepted for publication 6 November 2010.

*Junior Scientist, Institute of Propulsion Technology, Engine Acoustics, AT-TA, Müller-Breslau Strasse 8.

†Diploma Student, Institute of Propulsion Technology, Engine Acoustics, AT-TA, Müller-Breslau Strasse 8.

‡Scientist, Institute of Propulsion Technology, Engine Acoustics, AT-TA, Müller-Breslau Strasse 8.

§Professor, Institute of Propulsion Technology, Turbine, AT-TU, Bunsenstrasse 10.

¶Professor, Institute of Propulsion Technology, Engine Acoustics, AT-TA, Müller-Breslau Strasse 8.

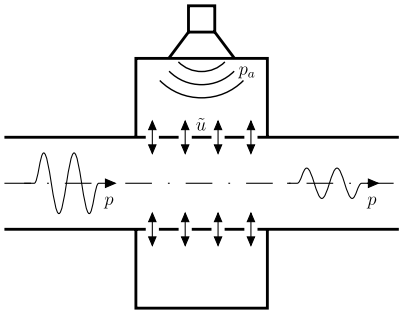

Fig. 1 Concept of the ZMFL. Illustration of an axisymmetric setup connected to a duct. The acoustic actuator generates a sound field p_a and induces an oscillating bias flow $\tilde{u}$, so that the sound wave p passing through the duct is attenuated.

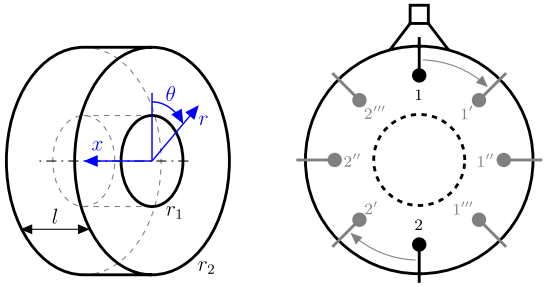

Fig. 2 Experimental setup of the ZMFL for the analysis of the sound field inside the annulus: dimensions and coordinate system (left) and microphone and loudspeaker positions (right).

phase relation. For the ZMFL the frequencies of the test signal and the actuator signal are different. Thus, the phase relation between these signals is of no importance, as signals of different frequencies do not have a fixed phase relation. The improved damping performance is not the result of an interference effect, but based on the ability of the actuator signal to produce an oscillating bias flow through the perforation of the liner.

This paper will examine the acoustic excitation of the ZMFL and its influence on the damping of the test signal. This will give a deeper insight into the complex physical phenomena. Furthermore, the resulting relations between the excitation and the damping performance will be incorporated in the development of an aeroacoustic actuator. Such a device could replace the loudspeaker in the ZMFL in industrial applications. The aeroacoustic actuator could be similar to a musical instrument, e.g., a flute or whistle, or as simple as a jet-edge configuration producing an edge-tone. Its advantage is that it does not contain any electronic or mechanical parts and is therefore suitable for the use in harsh environments. A typical application of the ZMFL could be the reduction of thermoacoustic instabilities in gas turbine combustors.

In a first step the sound field generated by the actuator inside the ZMFL will be analyzed in detail. Afterwards, the influence of the excited sound field on the damping performance will be studied. The main parameters are the actuator sound pressure level as well as the actuator frequency. The influence of mode structures evolving at certain frequencies will be looked at as well.

II. Analysis of Actuator Sound Field

To study the influence of the excitation on the damping performance the generated sound field needs to be analyzed first. The system consist of a loudspeaker connected to an annular cavity. Typical resonances are given by the boundaries of the cavity. The properties of the sound field at these resonances need to be determined.

A. Experimental Setup for Sound Field Analysis

The sound field analysis is done for the same ZMFL configuration used later for the damping measurements. A schematic drawing of the setup is shown in Fig. 2. A loudspeaker is connected to an annular cavity with a perforated inner wall. The dimensions of the annulus are: radius of the inner wall $r_1 = 71.25$ mm, radius of the outer wall $r_2 = 120$ mm, and length $l = 60$ mm. The perforated liner extends around the circumference at $r = r_1$ over the whole length l. It has an open-area ratio of 0.068 with circular apertures of 2.5 mm in diameter and a wall thickness of 1 mm. All other walls of the annulus are acoustically hard. The loudspeaker is connected to the cavity at $x = l/2$, $r = r_2$, and $\theta = 0°$ via an opening of 18 mm in diameter. Two microphones are installed flush in the sidewall at $x = 0$ and radius $r = 111$ mm, off-center between the outer wall and the liner. The sidewall including the microphones is able to rotate in θ direction in discrete steps of 45°. Therefore, the acoustic pressure can be acquired at eight azimuthal positions, while the loudspeaker is fixed at $\theta = 0°$. The relative positions are shown in Fig. 2. The microphones in this setup are only used for the analysis of the sound field and are not needed for the operation of the ZMFL.

The loudspeaker is a Monacor KU-516 speaker with a specified frequency range of 160–6500 Hz and a nominal power rating of 50 W. The excitation signal is provided by an Agilent 33220A function generator and amplified with a Dynacord L300 power amplifier. The microphones are $\frac{1}{4}$ in. G.R.A.S.-type 40BP condenser microphones. Their signals are recorded together with the loudspeaker input signal with an OROS OR36 data acquisition system at a sampling frequency of 16,384 Hz.

B. Sound Field Analysis

The sound field inside a cavity is affected by characteristic resonances. These resonances arise at certain frequencies depending on the geometry of the cavity and the acoustic properties of the boundaries. The geometry of our setup was given previously. For a theoretical analysis we consider all boundaries acoustically hard. Then, resonance frequencies can be calculated for each coordinate x, r, and θ based on the respective geometric constraints. The resonances in axial direction are based on the length l of the cavity. For a speed of sound $c = 343$ m/s they yield 2858 Hz for a $\lambda/2$ resonance and 5716 Hz for a λ resonance. The resonances in θ and r direction are given by the cuton frequencies of higher-order modes in azimuthal and radial direction. For acoustically hard walls the cuton frequencies of higher-order modes can be calculated from [18]

$$f^c_{(m,n)} = \sigma_{(m,n)} \frac{c}{2\pi r_2} \tag{1}$$

with the outer radius r_2, the speed of sound c, and the mode eigenvalue $\sigma_{(m,n)}$, where m and n correspond to the order of the azimuthal and radial mode, respectively. $\sigma_{(m,n)}$ are the eigenvalues of a characteristic function containing a sum of Bessel functions of the first and second kind. They are dependent on the ratio of the inner and outer radius of the annulus and the mode order (m, n). The values of $\sigma_{(m,n)}$ have been calculated with an in-house software tool. The resulting cuton frequencies for our geometry together with the associated acoustic pressure distribution are given in Fig. 3. The frequency range of interest for the following measurements is up to 3 kHz. There are five azimuthal and one axial resonance in that frequency range. The lowest radial resonance is already beyond this limit.

In this theoretical analysis it was assumed that all boundaries are acoustically hard. However, the ZMFL contains a perforated wall that violates this assumption. As the acoustic properties of the perforation are not known it is not possible to include it in the theoretical analysis. So, the resonances of the setup including the perforation are determined experimentally.

A sine sweep signal ranging from 200–8000 Hz is used and the acoustic pressure is measured at position 1 given in Fig. 2. This always coincides with a pressure maximum for all possible mode structures given in Fig. 3. For comparison with the theoretical findings and to reveal the influence of the perforation, a second measurement with only hard walls is made. For this second

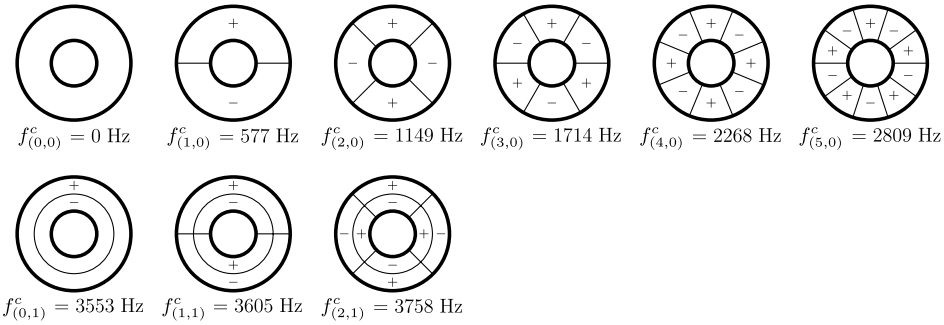

Fig. 3 Cuton frequencies $f^c_{(m,n)}$ and acoustic pressure distribution of the associated mode (m, n). Indicated are the azimuthal and radial nodal lines and the areas of positive and negative acoustic pressure at a particular time.

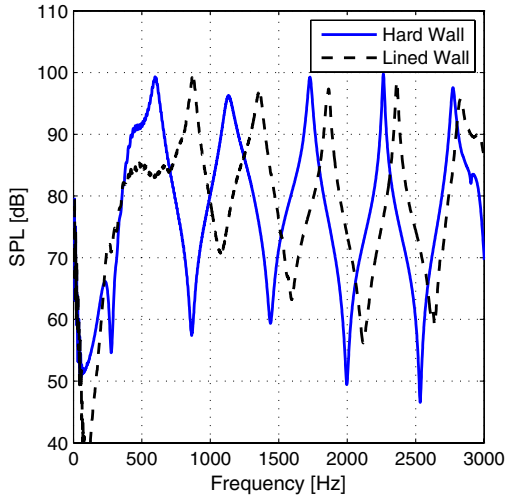

Fig. 4 Sound pressure spectra measured in the cavity of the ZMFL showing the influence of the lined wall on the frequencies of the resonances.

measurement the liner is replaced by a dummy liner without perforation. The resulting spectra of both configurations are shown in Fig. 4. The frequencies of the sound pressure maxima are listed in Table 1 together with the according frequencies from the theory. Both spectra show very dominant pressure maxima and minima at certain frequencies. The maxima identify the resonance frequencies. The measured frequencies of the hard wall case match with the azimuthal resonance frequencies found by the theory. The first axial resonance is determined to be at 2858 Hz and could be the cause of the minor irregularity in the spectra at about that position. Even though its influence is visible in the spectrum it is not nearly as strong as the azimuthal resonances. It is assumed that the resonances in the lined case originate from the same effect, only that they have been slightly shifted to higher frequencies due to the perforated inner wall. This offset is bigger for low frequencies and gets smaller for higher frequencies.

To confirm the mode structure in the lined wall case a mode analysis is performed. While the loudspeaker excites a resonance frequency found in the preceding measurements, two microphones

Table 1 Resonance frequencies of the cavity from measurements and theoretical considerations

Lined wall	Hard wall	
Measured, Hz	Measured, Hz	Theoretical, Hz
880	569	577
1355	1133	1149
1850	1728	1714
2360	2264	2268
2840	2773	2809

are used to acquire the acoustic pressure consecutively at all eight azimuthal positions given in Fig. 2. The data from all eight positions is used for the mode analysis. It is possible to resolve the first four azimuthal modes from the data at the eight positions. The mode $m = 5$ is not analyzed. The results are presented in Fig. 5. The mode analysis confirms the theoretical considerations. The sound field at the resonance frequencies is dominated by an azimuthal mode structure. The equal amplitude of the positive and negative mode of the same order suggests a standing wave pattern with pressure maxima and minima at fixed positions around the circumference. These structures are illustrated in Fig. 3 for the relevant modes.

III. Damping Measurements

Based on the findings in the previous section the influence of the sound field on the damping performance is studied. The ZMFL is installed in a duct acoustic test rig to perform the damping measurements. The test rig and the analysis method for the damping measurements are described in the following two sections, before the results are presented in Sec. III.C.

A. Experimental Setup for Damping Measurements

The ZMFL is installed in a duct acoustic test rig to perform damping measurements. A sketch of the test rig including the ZMFL is shown in Fig. 6. The Duct Acoustic Test Rig at DLR in Berlin allows high-precision acoustic measurements of the damping performance of various liner configurations. The test duct consists of two symmetric measurement sections (section 1 and section 2 in Fig. 6) of 1200 mm length each. They have a circular cross-sectional with a diameter of 140 mm. To minimize the reflection of sound at the end of the duct back into the measuring section the test duct is equipped with anechoic terminations at both ends (not shown in Fig. 6). Their specifications follow the International Standard ISO 5136:2003 standard [19].

A total of 12 microphones are mounted flush with the wall of the test duct. They are installed at different axial positions upstream and downstream of the damping module and are distributed exponentially with a higher density towards the damping module. Two microphones are installed opposite each other at the same axial position close to the signal source. As evanescent modes become more prominent in the vicinity of the source, their influence is reduced significantly by using the average value of these two microphones for the analysis. This technique helps to reduce the errors for frequencies approaching the cuton frequency of the first higher-order mode and thus, extends the frequency range for accurate results.

At the end of each section a loudspeaker is mounted at the circumference of the duct (*A* and *B* in Fig. 6). They deliver the test signal for the damping measurements. The signal used here is a multitone sine signal. It has been calibrated that each contained frequency generates an amplitude of about 102 dB inside the duct. The microphones used in these measurements are $\frac{1}{4}$ in. G.R.A.S.-type 40BP condenser microphones. Their signals are recorded with a 16-track OROS OR36 data acquisition system with a sampling frequency of 8192 Hz. The source signals for the loudspeakers are recorded on the remaining tracks. The test signal is produced by an

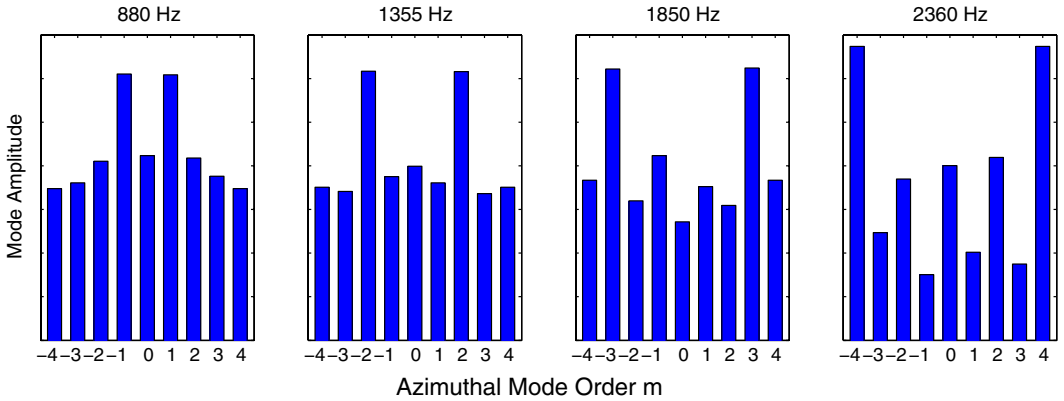

Fig. 5 Results of the mode analysis at the first four resonance frequencies.

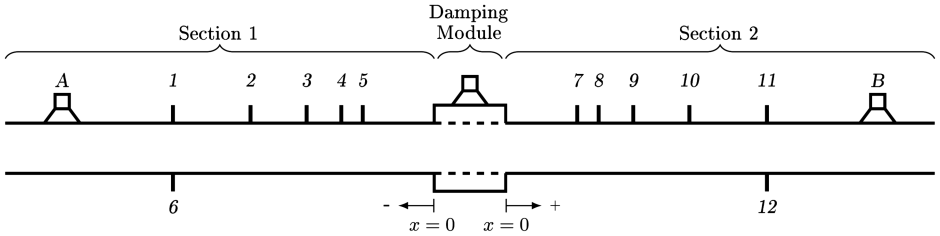

Fig. 6 Schematic setup of the duct acoustic test rig with speakers *A* and *B*, and microphones 1–12. The anechoic terminations at both ends are not shown.

Agilent 33220A function generator. The signals are fed through a Dynacord L300 amplifier before they power the Monacor KU-516 speakers. These loudspeakers have a specified frequency range of 160–6500 Hz and a nominal power rating of 50 W. This investigation is restricted to plane wave propagation inside the duct. The cuton frequency for the first higher-order mode is 1440 Hz. Accurate results are achieved up to 1350 Hz, beyond that limit the influence of evanescent modes increases the error rapidly. The lower frequency limit of 200 Hz is given by the resonance frequency of the loudspeakers. In the investigated frequency range the error of the results was successfully reduced to below 1%.

B. Analysis Method

The damping performance of the liner is evaluated using the dissipation coefficient. This is an integral value of the acoustic energy that is absorbed while a sound wave is passing the lined element.

The determination of the dissipation coefficient is based on a method proposed by Ronneberger [20] and contains a scattering-matrix approach as described by Åbom [21]. For each configuration two different sound fields are excited consecutively in two separate measurements (index a and b). Speaker A is used in the first measurement and in the second measurement the same signal is fed into speaker B. Then, the data of section 1 and section 2 (indexes 1 and 2) are analyzed separately. This results in four equations for the complex sound pressure amplitudes for each section and measurement:

$$\hat{p}_{1a}(x) = \hat{p}^{+}_{1a} e^{-ik_1^{+}x} + \hat{p}^{-}_{1a} e^{ik_1^{-}x} \tag{2}$$

$$\hat{p}_{2a}(x) = \hat{p}^{+}_{2a} e^{-ik_2^{+}x} + \hat{p}^{-}_{2a} e^{ik_2^{-}x} \tag{3}$$

$$\hat{p}_{1b}(x) = \hat{p}^{+}_{1b} e^{-ik_1^{+}x} + \hat{p}^{-}_{1b} e^{ik_1^{-}x} \tag{4}$$

$$\hat{p}_{2b}(x) = \hat{p}^{+}_{2b} e^{-ik_2^{+}x} + \hat{p}^{-}_{2b} e^{ik_2^{-}x} \tag{5}$$

$\hat{p}^{+}$ and $\hat{p}^{-}$ are the complex amplitudes of the downstream and upstream traveling waves with their respective wave numbers $k^{\pm}$.

The recorded microphone signals are transformed into the frequency domain using the method presented by Chung [22]. This method rejects uncorrelated noise, e.g., turbulent flow noise or other background noise, from the coherent sound pressure signals. Therefore, the sound pressure spectrum of one microphone is determined by calculating the cross-spectral densities between three signals, where one signal serves as a phase reference. In our case the phase reference signal is the source signal of the active loudspeaker. As a result we obtain a phase-correlated complex sound pressure spectrum for each microphone signal.

According to Eqs. (2–5) the measured acoustic signal is a superposition of two plane waves traveling in opposite direction. To determine the downstream and upstream propagating portions of the wave in each section, a mathematical model is fitted to the acoustic microphone data. This model considers viscous and thermal conductivity losses at the duct wall. They are included in the wave number with an attenuation factor α_w as proposed by Kirchhoff [23]:

$$\alpha_w = \frac{1}{Rc}\sqrt{\frac{\eta\omega}{2\rho}}\left(1 + \frac{\gamma - 1}{\sqrt{Pr}}\right) \tag{6}$$

with the duct radius R, the speed of sound c, the dynamic viscosity η, the angular frequency ω, the density of the fluid ρ, the ratio of the specific heat γ, and the Prandtl number Pr. As a result of this least-mean-square fit, the four complex sound pressure amplitudes $\hat{p}_1^{+}$, $\hat{p}_1^{-}$, $\hat{p}_2^{+}$ and $\hat{p}_2^{-}$ are identified at position $x = 0$ for both measurements. These sound pressure amplitudes are related to each other via the reflection and transmission coefficients of the test object. This is illustrated in Fig. 7 for the two different measurements a and b. To calculate the reflection and transmission coefficients r^{+}, r^{-}, t^{+}, and t^{-} from the sound pressure amplitudes the following four relations can be derived:

$$\hat{p}^{-}_{1a} = r^{+}\hat{p}^{+}_{1a} + t^{-}\hat{p}^{-}_{2a} \tag{7}$$

$$\hat{p}^{-}_{1b} = r^{+}\hat{p}^{+}_{1b} + t^{-}\hat{p}^{-}_{2b} \tag{8}$$

$$\hat{p}^{+}_{2a} = r^{-}\hat{p}^{-}_{2a} + t^{+}\hat{p}^{+}_{1a} \tag{9}$$

$$\hat{p}^{+}_{2b} = r^{-}\hat{p}^{-}_{2b} + t^{+}\hat{p}^{+}_{1b} \tag{10}$$

The equations from both measurements are combined and solved for the reflection and transmission coefficients. This results in

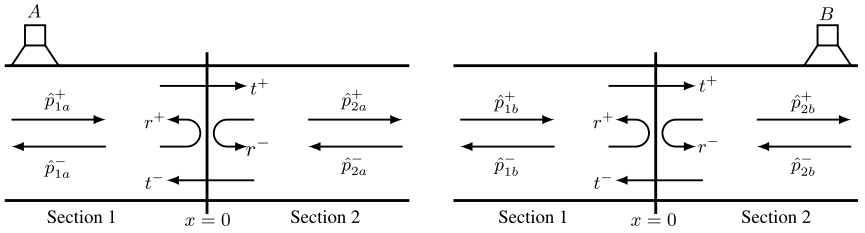

a) Sound field for upstream excitation **b) Sound field for downstream excitation**

Fig. 7 Illustration of the sound field in the duct by means of the sound pressure amplitudes $\hat{p}$, the reflection coefficient r and the transmission coefficient t: a) measurement a and b) measurement b.

$$r^+ = \frac{\hat{p}^-_{1a}\hat{p}^-_{2b} - \hat{p}^-_{1b}\hat{p}^-_{2a}}{\hat{p}^+_{1a}\hat{p}^-_{2b} - \hat{p}^+_{1b}\hat{p}^-_{2a}} \quad \text{and} \quad t^+ = \frac{\hat{p}^+_{2a}\hat{p}^-_{2b} - \hat{p}^+_{2b}\hat{p}^-_{2a}}{\hat{p}^+_{1a}\hat{p}^-_{2b} - \hat{p}^+_{1b}\hat{p}^-_{2a}} \tag{11}$$

for the downstream direction and accordingly for the upstream direction:

$$r^- = \frac{\hat{p}^+_{2b}\hat{p}^+_{1a} - \hat{p}^+_{2a}\hat{p}^+_{1b}}{\hat{p}^+_{1a}\hat{p}^-_{2b} - \hat{p}^+_{1b}\hat{p}^-_{2a}} \quad \text{and} \quad t^- = \frac{\hat{p}^+_{1a}\hat{p}^-_{1b} - \hat{p}^+_{1b}\hat{p}^-_{1a}}{\hat{p}^+_{1a}\hat{p}^-_{2b} - \hat{p}^+_{1b}\hat{p}^-_{2a}} \tag{12}$$

The advantage of combining the two measurements is that the resulting coefficients are independent from the reflections of sound at the duct terminations. These end-reflections are contained in the sound pressure amplitudes, but do not need to be calculated explicitly.

Based on the conservation of energy the dissipation of acoustic energy can be calculated directly from the reflection and transmission coefficients. To transform the pressure quantities p to energy quantities P the energy flux needs to be considered. Blokhintsev [24] defines the energy flux in a moving medium to

$$P^\pm = \frac{A}{2\rho c}(1 \pm M)^2 |\hat{p}^\pm|^2 \tag{13}$$

where A is the cross-sectional area of the duct and M is the Mach number of the flow. Hence, a sound wave propagating in flow direction is transmitting more energy than a wave traveling against the flow. This results in the following definition of the dissipation coefficient:

$$\Delta^\pm = 1 - \left(\frac{(1 \mp M)^2}{(1 \pm M)^2} \cdot |r^\pm|^2 + |t^\pm|^2 \right) \tag{14}$$

As the measurements in this study are done without mean flow in the duct, the results of the dissipation coefficient in positive and negative direction are identical. Therefore, only the results in positive direction will be presented later on.

C. Results of Damping Measurements

First some general remarks concerning the nomenclature: The excitation signal of the zero mass flow actuator is referred to as actuator signal with actuator sound pressure level and actuator frequency. The attenuated test signal in the duct is referred to as test signal with test signal sound pressure level and test signal frequency. The given values of the actuator sound pressure level are maximum values. They are measured at position 2 (see Fig. 2) in the cavity. At that position the sound pressure is always at maximum, independent of the mode structure.

The dependency of the damping performance of the ZMFL on the actuator sound pressure level is shown in Fig. 8. Plotted is the dissipation coefficient over the test signal frequency for several actuator sound pressure levels while the actuator frequency is kept constant at 880 Hz. It is obvious that the actuator sound pressure level is a crucial parameter. The damping improves considerably while increasing the actuator sound pressure level. Previous studies of a steady bias flow configuration [5] indicated an optimum bias flow velocity beyond which the damping was reduced again. Likewise there could be an optimum actuator sound pressure level at a given actuator frequency. However, this optimum is not reached yet in Fig. 8, but a saturation becomes visible towards the high sound pressure levels. It was not possible to produce higher sound pressure levels with the given speaker at that frequency.

Figure 9 illustrates the influence of the actuator frequency on the dissipation while the actuator sound pressure level is kept constant at 148 dB. The frequencies chosen for the actuator excitation are the resonance frequencies of the cavity. The resulting dissipation curves reveal a strong dependency of the damping performance on the actuator frequency. The damping declines for higher frequencies, settling at levels just slightly above the case without excitation in Fig. 8. For frequencies below the first resonance frequency it was not possible to reach comparable sound pressure levels with the given setup.

The general characteristic shape of the curves, mainly defined by the frequency of maximum dissipation, seems to be independent of the actuator sound pressure level or frequency. These parameters only influence the amount of dissipation. The characteristic shape seems to be bound to the geometric parameters of the perforation and the cavity. Figure 10 presents dissipation results of same liner geometry exposed to a steady bias flow of different velocities. In this case no actuator was used for additional excitation. The dissipation curves correspond to the ones obtained by the ZMFL. The characteristic shape is the same for both cases, the steady and unsteady bias flow. This confirms that the shape is defined by the geometry rather than the excitation. Furthermore, similar dissipation levels are achieved by the two different bias flow settings. The similarities of the results suggest that the underlying physical effects responsible for the absorption are the same in both cases.

As mentioned before, the frequencies chosen for the actuator are the resonance frequencies of the cavity. This proves to be convenient for reaching high sound pressure levels. The sound field at these frequencies is dominated by a pressure distribution defined by the respective mode. These pressure patterns have been illustrated in Fig. 3. The sound field in our case contains stationary nodal lines

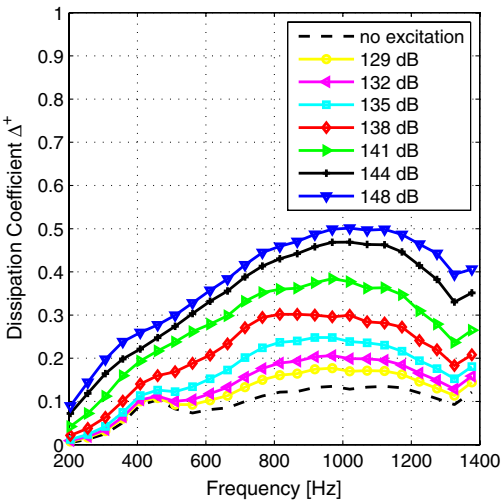

Fig. 8 Influence of the actuator sound pressure level on the damping performance of the ZMFL at a constant actuator frequency of 880 Hz.

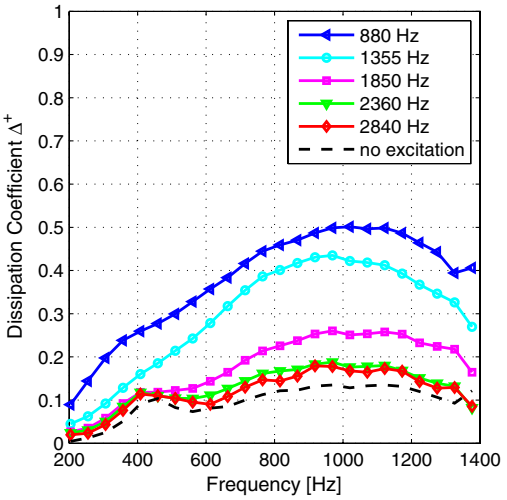

Fig. 9 Influence of the actuator frequency on the damping performance of the ZMFL at a constant actuator sound pressure level of 148 dB.

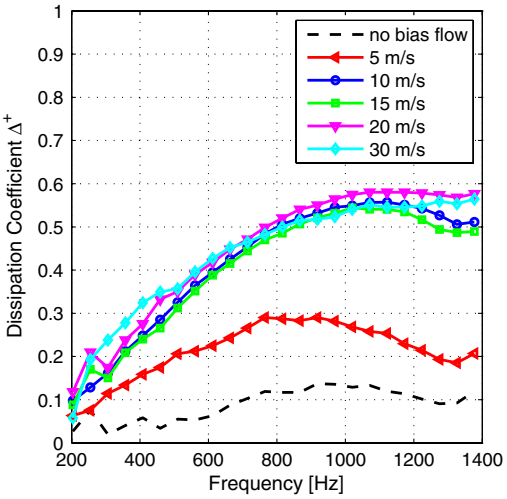

Fig. 10 Influence of a steady bias flow on the damping performance of a perforated liner without any actuator excitation.

where the pressure variation is at minimum. Following the assumption that a high-amplitude sound generates an oscillating bias flow leads to the conclusion that the areas around the nodal lines do not contribute to this effect. Further concluding that for a sound field with a distinct mode structure the damping performance is reduced due to this ineffective areas. This effect is independent of the mode order. Although modes of higher-order contain more nodal lines, the number of pressure maxima increases accordingly. In the end the area between a certain threshold stays the same. That means, a difference in damping performance is expected when comparing the results with a uniform pressure distribution ($m = 0$) to the results with a distinct mode structure ($m > 0$).

Hence, measurements are made to study the influence of this modal structure. A setup with two loudspeakers permits to either excite or suppress the mode structure at the cuton frequency of the first azimuthal mode. Therefore, an additional loudspeaker is mounted to the ZMFL. The second speaker is located exactly opposite to the first one at $\theta = 180°$. The phase of the two signals can be controlled independently. Operating the speakers in-phase ($\Delta\phi = 0°$) suppresses the development of the first azimuthal mode, while driving them in antiphase ($\Delta\phi = 180°$) condition intensifies the azimuthal structure. A mode analysis according to Sec. II.B is performed to verify the result of the excitation with the two speakers. The maximum sound pressure level is adjusted to 139.5 dB for both cases. The results are shown in Fig. 11. The desired sound fields could be excited accordingly. The in-phase excitation generates the

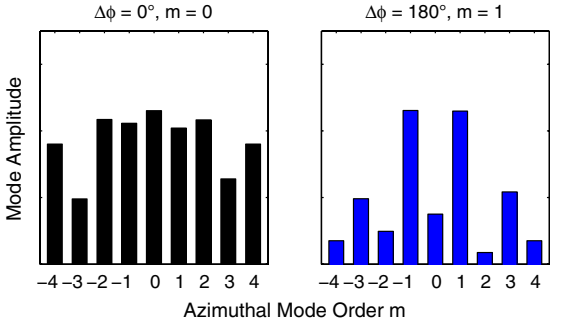

Fig. 11 Results of the mode analysis at $f^c_{(1,0)} = 880$ Hz for in-phase ($\Delta\phi = 0°$) and antiphase ($\Delta\phi = 180°$) excitation at constant maximum sound pressure level of 139.5 dB.

highest amplitude for $m = 0$, while $m = \pm 1$ dominates for the antiphase excitation.

The results of a damping measurement with these two excitations is presented in Fig. 12. As expected, the damping for $m = 0$ is slightly better than for $m = 1$. That confirms an influence of the nodal lines and suggests that they produce ineffective areas with respect to the damping.

The overall damping performance shown in Fig. 12 is not that good. To produce $m = 0$ the two speakers are working "against" each other as the sound field is aiming to $m = 1$. The input power of the speakers was considerably reduced exciting $m = 1$ with the same outcome of actuator sound pressure level. The next measurement should show that it is much more profitable to use the given resonance effects than trying to force a uniform pressure field. The

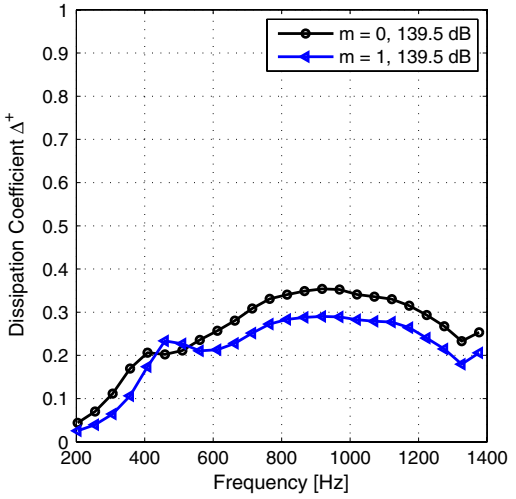

Fig. 12 Influence of the mode structure of the acoustic field inside the ZMFL on the damping performance at constant actuator frequency of 880 Hz and constant actuator sound pressure level of 139.5 dB.

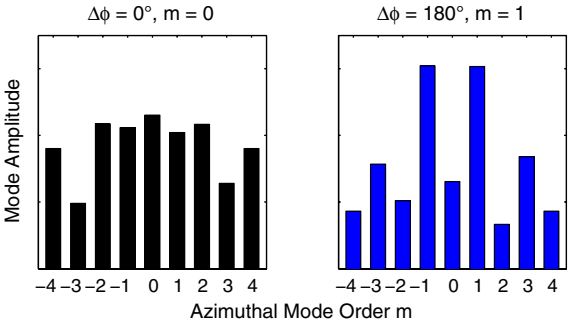

Fig. 13 Results of the mode analysis at $f^c_{(1,0)} = 880$ Hz for in-phase ($\Delta\phi = 0°$) and antiphase ($\Delta\phi = 180°$) excitation at constant power input into the loudspeakers.

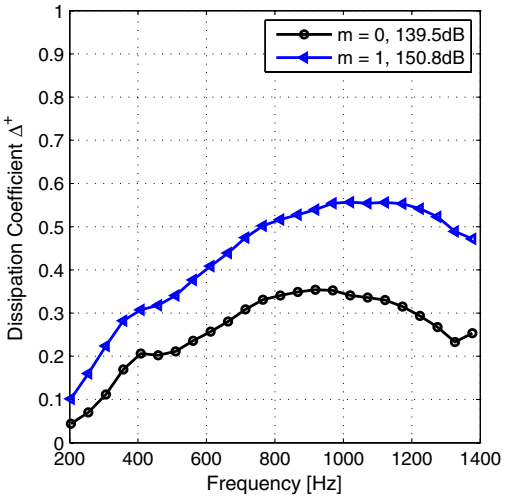

Fig. 14 Influence of the mode structure of the acoustic field inside the ZMFL on the damping performance at constant actuator frequency of 880 Hz and constant power input into the loudspeakers.

previous measurement of $m = 0$ is compared with a measurement with the same electrical input power into the speakers. The only difference between the two measurements is the phase relation between the loudspeakers. $\Delta\phi = 0°$ yields an actuator sound pressure level of 139.5 dB as seen before and $\Delta\phi = 180°$ results in a sound pressure level of 150.8 dB. The mode plots are shown in Fig. 13 and the respective dissipation curves are presented in Fig. 14. The difference is quite striking. The excitation with $m = 1$ at the same input power does not only catch up with the benefits of the uniform sound field at $m = 0$, but outperforms it immensely. It is of much greater benefit to use the resonance effect than trying to establish a uniform sound field.

IV. Conclusions

The sound field inside the ZMFL was studied in detail. The resonances occurring in the frequency range of interest were identified as cuton frequencies of azimuthal modes. This was confirmed by a mode analysis. The actuator sound pressure level and the actuator frequency show a strong influence on the damping performance. The damping improves for higher sound pressure levels, while it decreases for higher frequencies. A dependency of the damping on the dominant mode structure could be detected. However, this effect is overruled by the general positive influence at resonance by the generation of high sound pressure levels with little input power.

These findings will contribute to the development of an aeroacoustic actuator for the sound generation. The results have shown that it is of great benefit to use the resonance frequencies for the excitation. An aeroacoustic actuator naturally excites these cavity resonances of the system it is connected to. Such a setup yields high sound pressure levels, resulting in a excellent damping performance for a minimum of input power. The application of such an aeroacoustic actuator as the actuator in the ZMFL seems very promising.

References

[1] Dean, P. D., and Tester, B. J., "Duct Wall Impedance Control as an Advanced Concept for Acoustic Suppression," NASA CR-134998, 1975.

[2] Jing, X., and Sun, X., "Experimental Investigation of Perforated Liners with Bias Flow," *Journal of the Acoustical Society of America*, Vol. 106, No. 5, 1999, pp. 2436–2441. doi:10.1121/1.428128

[3] Follet, J. I., Betts, J. F., and Kelly, J. J., "Improvements to Acoustic Liner Broadband Absorption Using Bias Flow," 39th Aerospace Sciences Meeting and Exhibit, Reno, NV, AIAA Paper 2001-0823, 2001.

[4] Eldredge, J. D., and Dowling, A. P., "The Absorption of Axial Acoustic Waves by a Perforated Liner with Bias Flow," *Journal of Fluid Mechanics*, Vol. 485, 2003, pp. 307–335. doi:10.1017/S0022112003004518

[5] Heuwinkel, C., Enghardt, L., and Röhle, I., "Experimental Investigation of the Acoustic Damping of Perforated Liners with Bias Flow," 13th AIAA/CEAS Aeroacoustic Conference, Rome, AIAA Paper 2007-3525, 2007.

[6] Heuwinkel, C., Enghardt, L., and Röhle, I., "Concept and Experimental Investigation of a Zero Mass Flow Liner," 14th AIAA/CEAS Aeroacoustic Conference, Vancouver, AIAA Paper 2008-2931, 2008.

[7] Howe, M. S., "On the Theory of Unsteady High Reynolds Number Flow Through a Circular Aperture," *Proceedings of the Royal Society of London*, Vol. 366, No. 1725, 1979, pp. 205–223. doi:10.1098/rspa.1979.0048

[8] Bechert, D. W., "Sound Absorption Caused by Vorticity Shedding, Demonstrated with a Jet Flow," *Journal of Sound and Vibration*, Vol. 70, No. 3, 1980, pp. 389–405. doi:10.1016/0022-460X(80)90307-7

[9] Rienstra, S. W., "On the Acoustic Implications of Vortex Shedding from an Exhaust Pipe," *Journal of Engineering for Industry*, Vol. 103, No. 4, 1981, pp. 378–384. doi:10.1115/1.3184501

[10] Ingard, U., and Labate, S., "Acoustic Circulation Effects and the Nonlinear Impedance of Orifices," *Journal of the Acoustical Society of America*, Vol. 22, No. 2, 1950, pp. 211–218. doi:10.1121/1.1906591

[11] Ingard, U., and Ising, H., "Acoustic Nonlinearity of an Orifice," *Journal of the Acoustical Society of America*, Vol. 42, No. 1, 1967, pp. 6–17. doi:10.1121/1.1910576

[12] Whiffen, M. C., and Ahuja, K. K., "An Improved Schlieren System and Some New Results on Acoustically Excited Jets," *Journal of Sound and Vibration*, Vol. 86, No. 1, 1983, pp. 99–105. doi:10.1016/0022-460X(83)90946-X

[13] Salikuddin, M., and Brown, W. H., "Non-Linear Effects in Finite Amplitude Wave Propagation Through Ducts and Nozzles," *Journal of Sound and Vibration*, Vol. 106, No. 1, 1986, pp. 71–106. doi:10.1016/S0022-460X(86)80175-4

[14] Salikuddin, M., and Brown, W. H., "Non-Linear Effects in Finite Amplitude Propagation Through Orifice Plate and Perforated Plate Terminations," *Journal of Sound and Vibration*, Vol. 139, No. 3, 1990, pp. 383–405. doi:10.1016/0022-460X(90)90672-M

[15] Tam, C. K. W., and Kurbatskii, K. A., "Microfluid Dynamics and Acoustics of Resonant Liners," *AIAA Journal*, Vol. 38, No. 8, 2000, pp. 1331–1339. doi:10.2514/2.1132

[16] Tam, C. K. W., Kurbatskii, K. A., Ahuja, K. K., and R. J. Gaeta, J., "A Numerical and Experimental Investigation of the Dissipation Mechanisms of Resonant Acoustic Liners," *Journal of Sound and Vibration*, Vol. 245, No. 3, 2001, pp. 545–557. doi:10.1006/jsvi.2001.3571

[17] Glezer, A., and Amitay, M., "Synthetic Jets," *Annual Review of Fluid Mechanics*, Vol. 34, No. 1, 2002, pp. 503–529. doi:10.1146/annurev.fluid.34.090501.094913

[18] Tyler, J. M., and Sofrin, T. G., "Axial Flow Compressor Noise Studies," *SAE Transactions*, Vol. 70, 1962, pp. 309–332.

[19] "Acoustics: Determination of Sound Power Radiated into a Duct by Fans and Other Air-Moving Devices: In-Duct Method," International Organization for Standardization, Geneva, ISO 5136:2003, 2003.

[20] Ronneberger, D., *Genaue Messung der Schalldämpfung und der Phasengeschwindigkeit in durchströmten Rohren im Hinblick auf die Wechselwirkung zwischen Schall und Turbulenz*, Habilitationsschrift, Univ. of Göttingen, Göttingen, Germany, 1975.

[21] Åbom, M., "Measurement of the Scattering-Matrix of Acoustical Two-Ports," *Mechanical Systems and Signal Processing*, Vol. 5, No. 2, 1991, pp. 89–104. doi:10.1016/0888-3270(91)90017-Y

[22] Chung, J., "Rejection of Flow Noise Using a Coherence Function Method," *Journal of the Acoustical Society of America*, Vol. 62, No. 2, 1977, pp. 388–395. doi:10.1121/1.381537

[23] Kirchhoff, G., "Über den Einfluss der Wärmeleitung in einem Gase auf die Schallbewegung," *Annalen der Physik und Chemie*, Vol. 210, No. 6, 1868, pp. 177–193. doi:10.1002/andp.18682100602

[24] Blokhintsev, D. I., "Acoustics of a Nonhomogeneous Moving Medium," NACA TM 1399, 1946.

J. Astley
Associate Editor